Title: Blocking IRE1a;-endoribonuclease activity in hepatic stellate cells decreases tumor cell proliferation and metastasis in hepatocellular carcinoma

Authors: Natasa Pavlovic[1], Kessarin Thanapirom[3], Giuseppe Mazza[3], Krista Rombouts[3], Pär Gerwins[1,2] and Femke Heindryckx[1]

Affiliations:

(1) Department of Medical Cell Biology, Uppsala University, Uppsala, Sweden

(2) Department of Radiology, Uppsala University Hospital, Uppsala, Sweden

(3) Regenerative Medicine & Fibrosis Group, Institute for Liver and Digestive Health, University College London (UCL), London, UK

Running title: IRE1α-endoribonuclease activity in hepatocellular carcinoma

Keywords: Endoplasmic reticulum stress; fibrosis; hepatic stellate cells; IRE1α; tumor-stroma interactions;

Abbreviations: αSMA - α-smooth muscle actin; DEN – diethylnitrosamine; DMEM - Dulbecco modified eagle medium; ELISA - Enzyme-Linked immune Sorbent Assay, ER - Endoplasmic reticulum; FBS - fetal bovine serum; HCC - Hepatocellular carcinoma, H&E - Haematoxilin-eosin; TBS - tris-buffer saline; TGFβ - tumor growth factor β; UPR - unfolded protein response;

Corresponding author: Femke Heindryckx, Department of Medical Cell Biology, BOX 571, Husargatan 3, 75123 Uppsala, Sweden. Phone: +46768542025 Email: femke.heindryckx@mcb.uu.se

Document information:

Total document word count: 7072

Main body of text count: 4158

Number of figures: 7

Number of supplementary figures: 4

Number of supplementary tables: 1

Number of supplementary text files: 1

ABSTRACT

Hepatocellular carcinoma (HCC) is a primary liver tumor that arises in patients with liver cirrhosis. Activated stellate cells play an essential role in the pathogenesis of HCC. They are responsible for creating a fibrotic micro-environment and produce growth factors that enhance tumor cell proliferation and migration. In this study, mice were injected once per week with diethylnitrosamine to induce HCC in a background of chronic liver damage. Mice were treated with the specific IRE1α-ribonuclease inhibitor 4μ8C for 15 weeks, which led to a significant reduction in tumor burden and collagen deposition compared to untreated controls. Interactions between stellate cells and tumor cells were studied *in vitro* by co-culturing HCC-cell lines (HepG2 and Huh7) and hepatic stellate cells (LX2) using transwell co-culturing assays, 3D spheroids, 2D co-cultures and cell-engrafted human liver 3D-scaffolds. We found that tumor cells secrete factors that induce endoplasmic reticulum (ER)-stress in hepatic

stellate cells, which contributes to their activation. Inhibiting IRE1α-ribonuclease activity with 4μ8C or siRNA-transfection blocked stellate cell activation, which inhibited tumor cell proliferation and migration in different in vitro co-cultures. Our results suggest that IRE1α could be an important mediator in the communication between stellate cells and cancer cells and components of the ER-stress pathway may be therapeutically relevant for treating patients with HCC.

INTRODUCTION

Hepatocellular carcinoma (HCC) is a primary liver tumor that arises in a background of chronic liver disease. Activated stellate cells play an essential role in the pathogenesis of HCC by creating a fibrotic micro-environment that sustains tumor growth and by producing growth factors and cytokines that enhance tumor cell proliferation and migration[11, 14, 45]. One of the key players in the progression of cirrhosis to HCC is the hepatic stellate cell, which is activated during liver damage and differentiates towards a contractile myofibroblast-like cell.

Activated stellate cells play an essential role in the onset and progression of HCC and blocking their activation has been proposed as a potential therapy for patients with HCC [53]. Activated stellate cells drive tumor proliferation, mainly through the secretion of growth factors and cytokines [9]. They are also responsible for the deposition of extracellular matrix proteins, which can directly induce cellular transformation and alters the biophysical properties of the liver [52]. Tumor cells actively secrete growth factors, such as TGFβ and PDGF, which induce activation and migration of stellate cells, thereby creating a favorable tumor-environment [9, 35].

The unfolded protein response serves to cope with misfolded or unfolded proteins in the ER in an attempt to restore protein folding, increase ER-biosynthetic machinery and maintain cellular homeostasis[42]. It induces a cytoprotective effect by re-establishing cellular homeostasis and apoptotic signaling pathways can be activated in case of severe and/or prolonged ER-stress[46]. The presence of misfolded proteins is sensed via 3 transmembrane proteins in the ER: IRE1α, PERK and ATF6a. Actors of the ER-stress pathways have been described to play a role in the progression of

solid tumors, such as breast cancer[33], colon cancer [32] and HCC [50]. Activation of the UPR has also been implicated in the pathogenesis of non-alcoholic fatty liver disease[7, 28, 29], hepatitis B-induced carcinogenesis[30] and biliary cirrhosis[41]. We have previously shown that inhibiting the IRE1α-branch of the unfolded protein response (UPR) pathway using 4μ8C, blocks tumor growth factor-β (TGFβ)-induced activation of fibroblasts and stellate cells *in vitro* and reduces liver fibrosis *in vivo*[23]. In the current study, we define the role of ER-stress in the cross-talk between hepatic stellate cells and tumor cells in liver cancer, using different *in vivo* and *in vitro* models to study tumor-stroma interactions.

MATERIAL AND METHODS

Mouse model

A chemically induced mouse model for HCC was used, as previously described[20, 21]. Briefly, 5-week-old male sv129 mice received intraperitoneal injections once per week with 35mg/kg bodyweight DEN diluted in saline. From week 10, mice were injected twice per week with 10μg/g bodyweight 4μ8C (Sigma) in saline. After 25 weeks mice were euthanized and samples were taken for analysis. This method was approved by the Uppsala ethical committee for animal experimentation (C95/14). Each group contained 8 mice.

Cell culture and reagents

The HCC-cell lines (HepG2, ATCC and Huh7, kind gift from Dilruba Ahmed, Karolinska Institute) and HSC-line LX2 (Sigma-Aldrich, Darmstadt, Germany) were cultured at 37˚C with 5% CO_2 in Dulbecco modified eagle medium (DMEM) supplemented with 10% fetal bovine serum (FBS) (ThermoFisher, Stockholm,

Sweden). For starvation and stimulation no FBS was used. Cells were detached using trypsin-EDTA (ThermoFisher), re-suspended in growth medium and plated at a density of $5x10^3$ cells/cm^2. Cells were allowed to attach and left undisturbed for 8h before being starved for 16h. Afterwards, fresh starvation medium containing indicated growth factors or substances were added. Cells were exposed for 48h to 100µM 4µ8C (Sigma-Aldrich) or 10µM SB-431541 (Tocris, Abingdon, UK) as previously described[23]. For transwell co-culturing experiments, cells were grown on 12-well Corning Tissue Culture-plates with transwell inserts (Sigma-Aldrich) with 0,4µm-pore size, allowing the exchange of soluble factors, but preventing cell contact.

3D-tumor spheroids were generated on 96-well ultra-low attachment plates (Sigma-Aldrich)[10]. After 6 days, spheroids had reached approximately $1mm^2$ and 4µ8C was added. Proliferation was monitored during the subsequent 4 days. Tumor spheroids were retrieved from the plates after 10 days.

Fluorescent labeling of cells was done in imaging experiments by using CellTracker (ThermoFisher), according to manufacturer´s instructions. Cell pellets were incubated 30 minutes with 1µM of CellTracker™ Red CMTPX or 1µM of CellTracker™ Green CMFDA. Cells were washed twice in PBS prior to co-culturing.

Human liver scaffold decellularization and cell culture usage

Human healthy livers were obtained under the UCL Royal Free BioBank Ethical Review Committee (NRES Rec Reference: 11/WA/0077) approval. Informed consent was obtained for each donor and confirmed via the NHSBT ODT organ retrieval

pathway[37]. Liver 3D-scaffolds, were decellularized, sterilized and prepared for cell culture use as preciously described[37]. LX2 and HepG2-cells, as either mono-cultures or mixed co-culture, were released on top of each scaffold as $2.5*10^5$ cells in 20µL[48].

Proliferation

Cell proliferation was monitored via a resazurin reduction assay. A 1%-resazurin solution was added in 1/80 dilution to the cells and incubated for 24h, after which fluorescent signal was measured with a 540/35 excitation filter and a 590/20 emission filter on a Fluostar Omega plate reader.

Transfections

Nucleofection with 0,1µM siIRE1α (s200432, ThermoFisher), or 0,1 µM siCtrl (4390843, ThermoFisher) was done using Amaxa Nucleofector program S-005 in Ingenio electroporation solution (Mirus Bio LLC, Taastrup, Denmark).

Migration and chemotaxis

Non-directional migration was assessed using a scratch wound assay on fluorescently labelled LX2-cells and HepG2-cells. Scratch size was measured by analyzing light microscopy images in ImageJ, using the MRI Wound Healing Tool plug-in (http://dev.mri.cnrs.fr/projects/imagej-macros/wiki/Wound_Healing_Tool). Image analysis was done in ImageJ.

Directional migration was assessed using CellDirector-devices (GradienTech, Uppsala, Sweden). HepG2 and LX2-cells were labelled with CellTracker-dye and left to adhere overnight in the CellDirector-devices. Non-adherent cells were washed away with DMEM and cells were starved for 1h prior to commencing experiments. A

gradient of 0 to 10% FBS was created with a flow rate of 1.5 µl/minute. Cell movement was recorded using an Axiovision 200M microscope (Zeiss, Stockholm, Sweden) for 4h and tracked using Axiovision software (Zeiss). During the assay cells were kept at 37˚C with 5% CO_2.

Quantitative RT-PCR of mRNA

RNA was isolated from tissue or cell culture using the EZNA RNA isolation Kit (VWR, Spånga, Sweden) or using TRIzol reagent and RNeasy Universal Mini Kit (Qiagen, Sollentuna, Sweden) for human liver scaffolds[37]. RNA-concentration and purity were evaluated using Nanodrop. Afterwards, 500ng of mRNA was reverse transcribed using iScript cDNA synthesis kit (Bio-rad, Solna, Sweden). Amplifications were done using primers summarized in supplementary table 1. mRNA-expression was normalized to *18S, GAPDH* and/or *TBP1.* Fold change was calculated via the delta-delta-CT method.

The procedure to detect the spliced and unspliced isoforms of XBP1 was done by digesting RT-PCR product with the restriction enzyme *Pst*-I (ThermoFisher). This cleaves unspliced-XBP1 containing the Pst-I-cleavage site (CTGCA^G), but leaves the spliced isoform intact. The digestion reaction was stopped after 18h by 0,5M EDTA (pH 8.0) and run on a 1,5% agarose gel for 1h at 180V.

Stainings and immunocytochemistry

Tissue samples were fixed in 4% paraformaldehyde for 24h and subsequently embedded in paraffin. Cells and tumor spheroids were fixed for 10 minutes in 4% paraformaldehyde and stored at 4°C. Detailed staining protocols are provided as supplementary methods.

Enzyme-Linked immune Sorbent Assay (ELISA)

Medium samples from cells and from the engrafted scaffolds were used to measure TGFβ using ELISA (88-8350-22, ThermoFisher), following manufacturer´s guidelines.

Gene-set enrichment analysis

Gene expression profiles of HCC with a fibrous stroma and without fibrous stroma was accessed through PubMed´s Gene Expression Omnibus via accession number GSE31370[43]. A gene-set containing 79 proteins participating in the unfolded protein response was downloaded from The Harmonizome[40] and GSEA software was used to perform a gene-set enrichment assay[47].

Human protein atlas

Images from biopsies from HCC patients stained with antibodies against WIPI1[4], SHC1[3], PPP2R5B[2] and BiP[1] were obtained through the Human Protein Atlas[49].

Statistics

Data are presented as mean ± s.e.m. An unpaired, two-tailed Student's T-test was used to compare different groups; a $P<0.05$ was considered statistically significant. *In vitro* experiments were done in at least 3 independent replicates, *in vivo* experiments were done on at least 5 independent animals.

RESULTS

Pharmacological inhibition of IRE1α reduces tumor burden in a chemically induced mouse model for HCC

Hepatocellular carcinoma was induced in mice by weekly injections with diethylnitrosamine (DEN) for 25 weeks[20]. From week 10, the IRE1α-endonuclease activity was pharmacologically inhibited with 4μ8C. Histological analysis of liver tissue confirmed the presence of HCC and showed that 4μ8C significantly reduced number (Figure1A) and size (Figure1B) of tumors, leading to an overall decrease in tumor burden (Figure1C), as measured on H&E-stained liver slides (Figure1D). Stellate cell activation and liver fibrosis was quantified by Sirius Red staining (Figure 1E) and immunohistochemical staining with αSMA-antibodies (Figure 1F) on liver sections. Mice with HCC had a significant increase in the percentage of collagen (Figure 1E and G) and αSMA-staining (Figure 1F and H), compared to healthy mice. Treatment with 4μ8C restored collagen (Figure 1E and G) and αSMA-levels (Figure 1F and H) to a similar level as healthy livers. As a marker for (tumor) cell proliferation, PCNA-mRNA levels were determined on tumor nodules and surrounding non-tumor stromal tissue (Figure 1I). Proliferation was increased within the tumor, compared to healthy liver and stromal tissue. 4μ8C significantly decreased PCNA-mRNA-expression within the tumor, thus suggesting a decrease in tumor cell proliferation.

mRNA-levels of the ER-stress-chaperone BiP were measured in tumor and surrounding non-tumor cells (Supplementary figure 1A). BiP-mRNA-expression was increased in the surrounding non-tumor tissue of DEN-induced mice, while there was

no difference within the tumor, compared to healthy controls. Co-staining of liver tissue with αSMA and p-IRE1α-antibodies (Supplementary figure 1B and C) or BiP-antibodies (Supplementary figure 1D) in untreated mice with HCC, revealed that expression of ER-stress markers was mainly localized within activated stellate cells.

A gene-set enrichment assay on microarray data from HCC-patients with fibrotic septae and without fibrotic septae showed an increase of genes involved in the UPR in the fibrotic HCC samples (supplementary figure 2A). Several actors of the IRE1α-branch of the UPR are amongst the genes that contribute to the core-enrichment of this analysis (table 1). Immunohistochemical staining of liver biopsies from HCC-patients further confirmed presence of IRE1α-mediated ER-stress markers BiP, PPP2R5B, SHC1 and WIPI1 localized in the fibrotic scar tissue and near hepatic blood vessels (Supplementary figure 2B).

Tumor cells secrete factors that induce ER-stress in HSCs

Hepatic stellate cell-lines (LX2) and HCC-cell lines (HepG2 and Huh7) were grown in different compartments using a transwell assay. This confirmed that tumor cells secrete factors that increase mRNA-expression of CHOP (Figure 2A), spliced XBP1 (Figure 2B and D) and BiP (Figure 2C and H) in hepatic stellate cells co-cultured with tumor cells, indicating the presence of ER-stress. This also led to their activation, as measured by mRNA expression of αSMA (Figure 2F) and collagen (Figure 2G) in LX2-cells grown with HepG2 or Huh7 cells in a transwell assay. The mRNA-expression of αSMA and collagen was restored to baseline levels when 4μ8C was added to the transwell co-cultures. Tumor-spheroids containing HepG2 and LX2-cells were treated with 4μ8C, which led to a significant decrease in αSMA (Supplementary

figure 3A and B) and BiP (Supplementary figure 3C and D) as quantified by immunohistochemical staining.

De-cellularised human liver 3D-scaffolds were engrafted with HSCs (LX2) and tumor cells (HepG2). These scaffolds maintain the native bioactive 3D ECM-architecture of the liver donor and provide a physiologically and clinically relevant model to study cell-cell and cell-ECM interactions[36]. Sirius red staining and H&E staining confirmed that that LX2-cells and HepG2-cells successfully engrafted the collagen-rich matrix of the decellularized human liver scaffolds (Figure 3A). Surprisingly, stellate cell-activation markers αSMA (Figure 3B) and CTGF (Figure 3C) did not show significant differences between the conditions under investigation. However, engrafting both LX2-stellate cells and HepG2-cancer cells led to a significant increase of mRNA-expression of collagen, BiP and spliced XBP1 (Figure 3D) compared to scaffolds that were only engrafted with LX2-cells. Adding 4μ8C significantly decreased collagen and BiP-mRNA-expression in these LX2 and HepG2 co-cultured scaffolds, as seen on mRNA-expression (Figure 3D) and Sirius red stained slides (Figure5A).

Tumor cells are important sources of TGFβ, which is a known activator of stellate cells. Surprisingly, measuring TGFβ in mono-cultures lead to undetectable levels of TGFβ in Huh7-cells and low-levels in HepG2-cells (Supplementary figure 4A). These levels increased when LX2-cells were added to the co-cultures (Supplementary figure 4A). Engrafting both LX2-stellate cells and HepG2-cancer cells in the human liver scaffolds, slightly increased TGFβ-levels in the medium compared to scaffolds engrafted by only one cell type, but overall no significant differences were seen (Supplementary figure 4B). It is important to note that the baseline TGFβ-levels were markedly higher in the mono-cultured scaffolds, compared to the levels measured in cells grown in a standard 2D *in vitro* set-up (Supplementary figure 4A). Blocking

TGFβ-receptor signaling with SB-431541 significantly reduced mRNA-expression of ER-stress markers CHOP (Supplementary figure 3C), spliced XBP1 (Supplementary figure 4D-E) and BiP (Supplementary figure 4F) in stellate cells co-cultured with tumor cells using transwells. Adding a TGFβ-receptor-inhibitor to stellate cell – tumor cell co-cultures also reduced stellate cell activation, as measured by mRNA-expression of αSMA (Supplementary figure 4G) and collagen (Supplementary figure 4H). This indicates that TGFβ-secretion by tumor cells could be responsible for activating stellate cells and for inducing the UPR.

Pharmacological inhibition of IRE1α decreases tumor cell proliferation in stellate cell – tumor cell co-cultures

To study if activated stellate cells influence tumor cell behavior, we focused on two important hallmarks of cancer cells: proliferation and migration. In transwell co-culturing assays, we found that co-culturing HepG2 or Huh7-tumor cells with LX2-stellate cells significantly increased PCNA-mRNA-expression in HepG2 and Huh7-tumor cell lines (Figure 4A). Adding 4μ8C significantly decreased mRNA-expression of PCNA in Huh7-cells grown in a transwell co-culture with LX2-cells, while not affecting PCNA-expression in tumor cell mono-cultures (Figure 4A). PCNA-levels in HepG2-LX2 transwell co-cultures were slightly decreased, but this was not significant. Proliferation was measured 24h after exposure to 4μ8C in tumor cells (HepG2 and Huh7) grown as mono-cultures and in co-culture with LX2-stellate cells. While 4μ8C induced a significant increase in proliferation of HepG2-monocultures, no difference was seen in LX2-monocultures and a significant decrease was seen in the HepG2-LX2 co-cultures (Figure 4B). In the Huh7 tumor cell line, 4μ8C significantly decreased cell number compared to untreated controls and a similar reduction was

seen in the Huh7-LX2 co-cultures (Figure 4C). Immunohistochemical staining with antibodies against Epcam (tumor cells) and Ki67 (proliferation) clearly show that the effect on proliferation is mainly localized in the tumor cell population of these co-cultures (Figure 4D).

Since 2D-cultures fail to mimic physiological aspects of *in vivo* tumor growth, we used 3D-spheroids containing either tumor cells alone (HepG2 or Huh7) or in combination with LX2-cells to study cell proliferation. While the HepG2-spheroids experienced a lower proliferation rate when co-cultured with LX2 stellate cells (Figure 4E), there was no difference in proliferation between spheroid-monocultures and spheroid-co-cultures in the Huh7-cells (Figure 4F). Treatment with 4µ8C significantly decreased proliferation of the tumor spheroids consisting of tumor cells (Huh7 or HepG2) and stellate cells (LX2), while tumor spheroid monocultures were not affected by 4µ8C. Similarly, PCNA-mRNA-expression significantly increased in human liver scaffolds engrafted with HepG2 and LX2-cells, compared to those engrafted with only tumor cells (Figure 5A). Treatment with 4µ8C significantly decreased PCNA-mRNA-expression in the LX2+HepG2 liver scaffolds, whilst not affecting those engrafted with only tumor cells. This further confirms our hypothesis that 4µ8C affects tumor cell proliferation indirectly, namely by blocking the activation of stellate cells and thus impairing the interaction between tumor and stroma.

We measured the mRNA-expression of hepatocyte-nuclear-factor-4-alpha (Hnf4-α), which is associated with transcriptional regulation of genes implicated in lipid metabolism, glucose metabolism, differentiation and morphogenesis of hepatocytes and its presence predicts a favorable outcome for HCC[19]. While co-engraftment of LX2 and HepG2-cells in the liver scaffolds only lead to a marginal increase of Hnf4-α, treatment with 4µ8C significantly increased Hnf4-α-mRNA-expression, thus

suggesting an overall improvement of liver function and possibly improved prognosis (Figure 5B). Immunohistochemical staining of Epcam and ki67, showed that the HCC-cells have successfully engrafted the entire surface of the scaffolds and that 4µ8C decreases proliferation (Figure 5C).

Pharmacological inhibition of IRE1α decreases tumor cell migration in stellate cell – tumor cell co-cultures

Stellate cells play a pivotal role in inducing a pro-metastatic phenotype and directing cell migration[45]. In the transwell co-culturing assay, we found that co-culturing HepG2 and Huh7-tumor cells with LX2-cells, significantly increased mRNA-expression of the pro-metastatic marker MMP9 in HepG2-cells (Figure 6A) and MMP1 in HepG2 and Huh7-cells (Figure 6B). Adding 4µ8C significantly decreased the mRNA-expression of MMP1 in HepG2+LX2 and Huh7+LX2 transwell co-cultures, while a non-significant decrease of MMP9 mRNA-expression was seen in Huh7+LX2 transwell co-cultures. To assess whether this reduction in mRNA-expression of pro-metastatic markers has a functional effect on cell migration, a scratch wound assay was performed on confluent monolayers of mono-cultures (HepG2 or LX2) or tumor cell (HepG2) – stellate cell (LX2) co-cultures (Figure 6C). To visualize closing of the scratch wound by each individual cell type, cells were fluorescently labeled using CellTracker Green (tumor cells) or CellTracker Red (LX2 stellate cells) (Figure 6D). Tumor-stellate cell co-cultures were the most efficient to close the scratch wound (Figure 6E). This was significantly inhibited when co-cultures were treated with 4µ8C. We also observed a direct effect of 4µ8C on LX2 and HepG2-migration, since treatment with 4µ8C lead to a significant reduction in wound closure after 24h, compared to untreated controls. It is important to note that traditional scratch wound assays cannot distinguish between

proliferation and migration[13]. Considering that we observed a direct effect of 4μ8C on cell proliferation in HepG2-monocultures, this could have interfered with the quantification of wound closure. To overcome this limitation, we counted the individual number of cells in the middle of the wound area (Figure 6F and G). Since these cells are not at the edge of the scratch, it is more likely that they have actively migrated and are not merely a result of proliferation[8]. No significant difference was seen between HepG2 or LX2-cells within the wound area of HepG2-LX2 co-cultures after 24 hours (Figure9F). However, 4μ8C-treatment significantly decreased migration of HepG2-cells and LX2-cells inside the scratch wound in co-cultures, while not affecting mono-cultures (Figure 6G).

Metastasis is usually a result of directed migration and chemotaxis toward physical and biochemical gradients within the tumor stroma[38]. We used a microfluidic-based device for studying cell migration towards a stable gradient of chemotactic factors, such as FBS. 4μ8C significantly decreased total migration (Supplementary figure 5A-C) and directional migration towards FBS (Supplementary figure 5B and D) of HepG2-cells co-cultured with LX2-cells. Similarly, inhibition of ER-stress with 4μ8C significantly decreased total migration (Supplementary figure 5E and G) and directional migration towards FBS (Supplementary figure 5F and H) of LX2-cells co-cultured with HepG2-cells. Overall, these data suggest that stellate cells increase proliferation and pro-metastatic potential of tumor cells and blocking the IRE1α-RNase activity decreases tumor cell proliferation and migration.

Silencing of IRE1α in stellate cells decreases tumor cell proliferation and migration in co-cultures

To investigate whether the effect of blocking IRE1α is due to a direct effect on the tumor cells or because of an indirect effect via stellate cells, we transfected the stellate-line LX2 with an IRE1α-siRNA prior to co-culturing them in a transwell assay with HepG2-cells. Transfection efficiency was determined via qPCR and showed a 50% reduction in the IRE1α-mRNA-expression (Figure 7A) compared to non-transfected (Ctrl) or mock-transfected (Scr) controls. In the transwell co-culturing assay, we found that silencing IRE1α in the LX2-cells significantly decreased PCNA-mRNA-expression in HepG2-cells (Figure 7B). Silencing IRE1α in the LX2-cells lead to a significant reduction of proliferation in LX2-HepG2 co-cultures (Figure 7C) and LX2-HepG2 spheroids (Figure 7D). Immunocytochemical staining with αSMA-antibodies (Figure 7E), confirmed a significant reduction of αSMA after si-IRE1α-transfection of LX2-stellate cells in HepG2-LX2 spheroid co-cultures (Figure 7F). A scratch wound assay on HepG2-LX2 co-cultures verified that silencing of IRE1α in LX2-cells significantly reduced wound closure compared to non-transfected and mock-transfected stellate cells (Figure 7G - H). Overall, these data confirm that blocking the IRE1α-pathway in HSCs decreases proliferation and pro-metastatic potential of tumor cells.

DISCUSSION

There is increasing evidence that ER-stress and activation of the UPR play an essential role during hepatic inflammation and chronic liver disease. We have previously shown that inhibition of IRE1α prevents stellate cell activation and reduces liver cirrhosis *in vivo*[23]. In this report, we further define a role of ER-stress and the UPR in the interaction between tumor cells and HSCs and show IRE1α could form a

valuable therapeutic target to slow down the progression of hepatocellular carcinoma.

Activated stellate cells play an important role in promoting tumorigenesis and tumors are known to secrete cytokines such as TGFβ, which induce myofibroblast activation and creates an environment that sustains tumor growth[22]. Since over 80% of HCC arises in a setting of chronic inflammation associated with liver fibrosis, targeting the fibrotic tumor micro-environment is often proposed as a valuable therapeutic strategy for HCC-patients [14]. We and others have shown that ER-stress plays an important role in stellate cell activation and contributes to the progression of liver fibrosis [23-26]. The mechanisms by which the UPR promotes stellate cell activation have been attributed to regulating the expression of c-MYB[23], increasing the expression of SMAD-proteins[26] and/or by triggering autophagy[25].

In our study, we show that ER-stress plays an important role in stellate cell – tumor cell interactions and that pharmacological inhibition of IRE1α-endoribonuclease activity slows down the progression of HCC *in vivo*. We demonstrate that tumor cells induce ER-stress in HSCs, thereby contributing to their activation and creating an environment that is supportive for tumor growth and metastasis. Activated stellate cells are known to enhance migration and proliferation of tumor cells *in vitro*[45] and *in vivo*[5], possibly by producing extracellular matrix proteins and by producing growth factors. Extracellular matrix proteins such as collagen can act as a scaffold for tumor cell migration[18], alter the expression of MMP´s[45] and induce epithelial-mesenchymal transition[27]. Activated stellate cells are also an important source of hepatocyte growth factor, which promotes proliferation, cell invasion and epithelial-mesenchymal

transition via the c-MET signaling pathway[34]. Interestingly, blocking ER-stress in the stellate cell population reduced tumor-induced activation towards myofibroblasts, which then decreases proliferation and migration of tumor-cells in co-cultures. This suggests that targeting the microenvironment using an ER-stress inhibitor could be a promising strategy for patients with HCC.

It is important to note that we cannot exclude a direct effect of 4μ8C on tumor cells. The UPR has been described as an essential hallmark of HCC[44], although its role within tumorigenesis remains controversial[50]. While a mild to moderate level to ER-stress leads to activation of the UPR and enables cancer cells to survive and adapt to adverse environmental conditions, the occurrence of severe or sustained ER-stress leads to apoptosis. Both ER-stress inhibitors as ER-stress inducers have therefore been shown to act as potential anti-cancer therapies[12]. A recent study by Wu *et al*, demonstrated that IRE1α promotes progression of HCC and that hepatocyte specific ablation of IRE1α results in a decreased tumorigenesis[51]. In contrast to their study, we found a greater upregulation of actors of the IRE1α-branch within the stroma than in the tumor itself and identified that expression of ER-stress markers was mainly localized within the HSC-population. An important difference between both studies is the mouse model. While Wu *et al* used a single injection of DEN, we performed weekly injections, causing tumors to occur in a background of fibrosis[20]. Our *in vitro* studies with mono-cultures confirm that 4μ8C also has a direct effect on proliferation and migration of HCC cells – similar to the findings of Wu *et al* - and the response depends on the tumor cell line. Adding 4μ8C to HepG2-cells significantly increased proliferation, while a significant decrease was seen in the Huh7-cells. This difference in response could be due IRE1α´s function as a key cell

fate regulator. On the one hand it can induce mechanisms that restore protein homeostasis and promote cytoprotection, while on the other hand IRE1α also activates apoptotic signaling pathways. How and when IRE1α exerts its cytoprotective or its pro-apoptotic function remains largely unknown. The duration and severity of ER-stress seems to be a major contributor to the switch towards apoptosis, possibly by inducing changes in the conformational structure of IRE1α[17]. The threshold at which cells experience a severe and prolonged ER-stress that would induce apoptosis could differ between different cell lines, depending on the translational capacity of the cells (e.g. ER-size, number of chaperones and the amount of degradation machinery) and the intrinsic sources that cause ER-stress [15]. A study of Li *et al*, has specifically looked at how IRE1α regulates cell growth and apoptosis in HepG2-cells[31]. Similar to our findings, they discovered that inhibiting IRE1α enhances cell proliferation, while over-expression of IRE1α increases the expression of polo-like kinase, which leads to apoptosis. Interestingly, polo-like kinases have divergent roles on HCC-cell growth depending on which cell line is used, which could explain the different response to 4μ8C in Huh7 and HepG2-cells [39]. Studies on glioma cells show that IRE1α regulates invasion through MMP´s[6]. In line with these results, we also detected a reduction of MMP1-mRNA expression after 4μ8C-treatment and observed a direct effect on wound closure in HepG2-cells. These results indicate that ER-stress could play a direct role in regulating tumor cell invasion, in addition to its indirect effect via stellate cells.

In conclusion, the aim of this study was to define the role of ER-stress in the cross-talk between HSCs and tumor cells in liver cancer. We show that pharmacologic inhibition of the IRE1α-signaling pathway decreases tumor burden in a DEN-induced

mouse model for HCC. Using several *in vitro* 2D and 3D co-culturing methods, we identified that tumor cells induce ER-stress in HSCs and that this contributes to their activation. Blocking ER-stress in these HSCs prevents their activation, which then decreases proliferation and migration of tumor cells.

ACKNOWLEDGEMENTS

This research was funded through grants obtained from the Swedish Cancer Foundation (Cancerfonden, CAN2017/518 and CAN2013/1273), The Swedish children's cancer foundation (Barncancerfonden), the Swedish society for medical research (SSMF, S17-0092), the O.E. och Edla Johanssons stiftelse. These funding sources were not involved in the study design; collection, analysis and interpretation of data; writing of the report; and in the decision to submit the article for publication. We would like to thank visiting students Kim Vanhollebeke and Justine Dobbelaere for their technical assistance; GradienTech for providing us with their CellDirector assays and Paul O´Callaghan for his valuable input on our project.

Competing interest: The authors have no conflict of interest to report.

REFERENCES

1 https://www.proteinatlas.org/ENSG00000044574-HSPA5/pathology/liver+cancer. The Human Protein Atlas V19.

2 https://www.proteinatlas.org/ENSG00000068971-PPP2R5B/pathology/liver+cancer#imid_9419368. The Human Protein Atlas V19.

3 https://www.proteinatlas.org/ENSG00000160691-SHC1/pathology/liver+cancer. The Human Protein Atlas V19.

4 https://www.proteinatlas.org/ENSG00000070540-WIPI1/pathology/liver+cancer.doi: . The Human Protein Atlas 2019; V19.

5 Amann T, Bataille F, Spruss T, Muhlbauer M, Gabele E, Scholmerich J *et al*. Activated hepatic stellate cells promote tumorigenicity of hepatocellular carcinoma. Cancer Sci 2009; 100: 646-653.

6 Auf G, Jabouille A, Guerit S, Pineau R, Delugin M, Bouchecareilh M *et al*. Inositol-requiring enzyme 1alpha is a key regulator of angiogenesis and invasion in malignant glioma. Proceedings of the National Academy of Sciences of the United States of America 2010; 107: 15553-15558.

7 Bandla H, Dasgupta D, Mauer AS, Nozickova B, Kumar S, Hirsova P *et al*. Deletion of endoplasmic reticulum stress-responsive co-chaperone p58(IPK) protects mice from diet-induced steatohepatitis. Hepatology research : the official journal of the Japan Society of Hepatology 2018.

8 Bise R, Kanade T, Yin Z, Huh SI. Automatic cell tracking applied to analysis of cell migration in wound healing assay. Conf Proc IEEE Eng Med Biol Soc 2011; 2011: 6174-6179.

9 Caja L, Dituri F, Mancarella S, Caballero-Diaz D, Moustakas A, Giannelli G *et al*. TGF-beta and the Tissue Microenvironment: Relevance in Fibrosis and Cancer. Int J Mol Sci 2018; 19.

10 Calitz C, Hamman JH, Fey SJ, Viljoen AM, Gouws C, Wrzesinski K. A sub-chronic Xysmalobium undulatum hepatotoxicity investigation in HepG2/C3A spheroid cultures compared to an in vivo model. J Ethnopharmacol 2019; 239: 111897.

11 Carloni V, Luong TV, Rombouts K. Hepatic stellate cells and extracellular matrix in hepatocellular carcinoma: more complicated than ever. Liver international : official journal of the International Association for the Study of the Liver 2014.

12 Corazzari M, Gagliardi M, Fimia GM, Piacentini M. Endoplasmic Reticulum Stress, Unfolded Protein Response, and Cancer Cell Fate. Front Oncol 2017; 7: 78.

13 Cormier N, Yeo A, Fiorentino E, Paxson J. Optimization of the Wound Scratch Assay to Detect Changes in Murine Mesenchymal Stromal Cell Migration After Damage by Soluble Cigarette Smoke Extract. J Vis Exp 2015: e53414.

14 Coulouarn C, Clement B. Stellate cells and the development of liver cancer: therapeutic potential of targeting the stroma. J Hepatol 2014; 60: 1306-1309.

15 Cubillos-Ruiz JR, Bettigole SE, Glimcher LH. Tumorigenic and Immunosuppressive Effects of Endoplasmic Reticulum Stress in Cancer. Cell 2017; 168: 692-706.

16 Duval K, Grover H, Han LH, Mou Y, Pegoraro AF, Fredberg J *et al*. Modeling Physiological Events in 2D vs. 3D Cell Culture. Physiology (Bethesda) 2017; 32: 266-277.

17 Ghosh R, Wang L, Wang ES, Perera BG, Igbaria A, Morita S *et al*. Allosteric inhibition of the IRE1alpha RNase preserves cell viability and function during endoplasmic reticulum stress. Cell 2014; 158: 534-548.

18 Han W, Chen S, Yuan W, Fan Q, Tian J, Wang X *et al*. Oriented collagen fibers direct tumor cell intravasation. Proceedings of the National Academy of Sciences of the United States of America 2016; 113: 11208-11213.

19 Hang HL, Liu XY, Wang HT, Xu N, Bian JM, Zhang JJ *et al*. Hepatocyte nuclear factor 4A improves hepatic differentiation of immortalized adult human hepatocytes and improves liver function and survival. Experimental cell research 2017; 360: 81-93.

20 Heindryckx F, Mertens K, Charette N, Vandeghinste B, Casteleyn C, Van Steenkiste C *et al*. Kinetics of angiogenic changes in a new mouse model for hepatocellular carcinoma. Mol Cancer 2010; 9: 219.

21 Heindryckx F, Bogaerts E, Coulon SH, Devlies H, Geerts AM, Libbrecht L *et al*. Inhibition of the placental growth factor decreases burden of cholangiocarcinoma and hepatocellular carcinoma in a transgenic mouse model. Eur J Gastroenterol Hepatol 2012; 24: 1020-1032.

22 Heindryckx F, Gerwins P. Targeting the tumor stroma in hepatocellular carcinoma. World J Hepatol 2015; 7: 165-176.

23 Heindryckx F, Binet F, Ponticos M, Rombouts K, Lau J, Kreuger J *et al*. Endoplasmic reticulum stress enhances fibrosis through IRE1alpha-mediated degradation of miR-150 and XBP-1 splicing. EMBO Mol Med 2016; 8: 729-744.

24 Hernandez-Gea V, Hilscher M, Rozenfeld R, Lim MP, Nieto N, Werner S *et al*. Endoplasmic reticulum stress induces fibrogenic activity in hepatic stellate cells through autophagy. Journal of hepatology 2013; 59: 98-104.

25 Kim RS, Hasegawa D, Goossens N, Tsuchida T, Athwal V, Sun X *et al*. The XBP1 Arm of the Unfolded Protein Response Induces Fibrogenic Activity in Hepatic Stellate Cells Through Autophagy. Sci Rep 2016; 6: 39342.

26 Koo JH, Lee HJ, Kim W, Kim SG. Endoplasmic Reticulum Stress in Hepatic Stellate Cells Promotes Liver Fibrosis via PERK-Mediated Degradation of HNRNPA1 and Up-regulation of SMAD2. Gastroenterology 2016; 150: 181-193 e188.

27 Kumar S, Das A, Sen S. Extracellular matrix density promotes EMT by weakening cell-cell adhesions. Mol Biosyst 2014; 10: 838-850.

28 Kwanten WJ, Vandewynckel YP, Martinet W, De Winter BY, Michielsen PP, Van Hoof VO *et al*. Hepatocellular autophagy modulates the unfolded protein response and fasting-induced steatosis in mice. American journal of physiology Gastrointestinal and liver physiology 2016; 311: G599-G609.

29 Lebeaupin C, Vallee D, Hazari Y, Hetz C, Chevet E, Bailly-Maitre B. Endoplasmic reticulum stress signalling and the pathogenesis of non-alcoholic fatty liver disease. Journal of hepatology 2018; 69: 927-947.

30 Li J, He J, Fu Y, Hu X, Sun LQ, Huang Y *et al*. Hepatitis B virus X protein inhibits apoptosis by modulating endoplasmic reticulum stress response. Oncotarget 2017; 8: 96027-96034.

31 Li X, Zhu H, Huang H, Jiang R, Zhao W, Liu Y *et al.* Study on the effect of IRE1a on cell growth and apoptosis via modulation PLK1 in ER stress response. Molecular and cellular biochemistry 2012; 365: 99-108.

32 Li XX, Zhang HS, Xu YM, Zhang RJ, Chen Y, Fan L *et al*. Knockdown of IRE1alpha inhibits colonic tumorigenesis through decreasing beta-catenin and IRE1alpha targeting suppresses colon cancer cells. Oncogene 2017; 36: 6738-6746.

33 Liang H, Xiao J, Zhou Z, Wu J, Ge F, Li Z *et al*. Hypoxia induces miR-153 through the IRE1alpha-XBP1 pathway to fine tune the HIF1alpha/VEGFA axis in breast cancer angiogenesis. Oncogene 2018.

34 Liu WT, Jing YY, Yu GF, Chen H, Han ZP, Yu DD *et al*. Hepatic stellate cell promoted hepatoma cell invasion via the HGF/c-Met signaling pathway regulated by p53. Cell Cycle 2016; 15: 886-894.

35 Lu Y, Lin N, Chen Z, Xu R. Hypoxia-induced secretion of platelet-derived growth factor-BB by hepatocellular carcinoma cells increases activated hepatic stellate cell proliferation, migration and expression of vascular endothelial growth factor-A. Mol Med Rep 2015; 11: 691-697.

36 Mazza G, Rombouts K, Rennie Hall A, Urbani L, Vinh Luong T, Al-Akkad W *et al*. Decellularized human liver as a natural 3D-scaffold for liver bioengineering and transplantation. Sci Rep 2015; 5: 13079.

37 Mazza G, Al-Akkad W, Telese A, Longato L, Urbani L, Robinson B *et al.* Rapid production of human liver scaffolds for functional tissue engineering by high shear stress oscillation-decellularization. Sci Rep 2017; 7: 5534.

38 Oudin MJ, Weaver VM. Physical and Chemical Gradients in the Tumor Microenvironment Regulate Tumor Cell Invasion, Migration, and Metastasis. Cold Spring Harb Symp Quant Biol 2016; 81: 189-205.

39 Pellegrino R, Calvisi DF, Ladu S, Ehemann V, Staniscia T, Evert M *et al*. Oncogenic and tumor suppressive roles of polo-like kinases in human hepatocellular carcinoma. Hepatology 2010; 51: 857-868.

40 Rouillard AD, Gundersen GW, Fernandez NF, Wang Z, Monteiro CD, McDermott MG *et al*. The harmonizome: a collection of processed datasets gathered to serve and mine knowledge about genes and proteins. Database (Oxford) 2016; 2016.

41 Sasaki M, Yoshimura-Miyakoshi M, Sato Y, Nakanuma Y. A possible involvement of endoplasmic reticulum stress in biliary epithelial autophagy and senescence in primary biliary cirrhosis. J Gastroenterol 2015; 50: 984-995.

42 Schroder M, Kaufman RJ. ER stress and the unfolded protein response. Mutat Res-Fund Mol M 2005; 569: 29-63.

43 Seok JY, Na DC, Woo HG, Roncalli M, Kwon SM, Yoo JE *et al*. A fibrous stromal component in hepatocellular carcinoma reveals a cholangiocarcinoma-like gene expression trait and epithelial-mesenchymal transition. Hepatology 2012; 55: 1776-1786.

44 Shuda M, Kondoh N, Imazeki N, Tanaka K, Okada T, Mori K *et al*. Activation of the ATF6, XBP1 and grp78 genes in human hepatocellular carcinoma: a possible involvement of the ER stress pathway in hepatocarcinogenesis. Journal of hepatology 2003; 38: 605-614.

45 Song Y, Kim SH, Kim KM, Choi EK, Kim J, Seo HR. Activated hepatic stellate cells play pivotal roles in hepatocellular carcinoma cell chemoresistance and migration in multicellular tumor spheroids. Sci Rep 2016; 6: 36750.

46 Sovolyova N, Healy S, Samali A, Logue SE. Stressed to death - mechanisms of ER stress-induced cell death. Biol Chem 2014; 395: 1-13.

47 Subramanian A, Tamayo P, Mootha VK, Mukherjee S, Ebert BL, Gillette MA *et al*. Gene set enrichment analysis: a knowledge-based approach for interpreting genome-wide expression profiles. Proc Natl Acad Sci U S A 2005; 102: 15545-15550.

48 Thanapirom K, Frenguelli L, Al-Akkad W, Zhang ZZ, Pinzani M, Mazza G *et al*. Optimization and validation of a novel three-dimensional co-culture system in decellularized human liver scaffold for the study of liver fibrosis and cancer. Journal of hepatology 2019; 70: E24-E24.

49 Uhlen M, Fagerberg L, Hallstrom BM, Lindskog C, Oksvold P, Mardinoglu A *et al*. Proteomics. Tissue-based map of the human proteome. Science 2015; 347: 1260419.

50 Vandewynckel YP, Laukens D, Geerts A, Bogaerts E, Paridaens A, Verhelst X *et al*. The paradox of the unfolded protein response in cancer. Anticancer Res 2013; 33: 4683-4694.

51 Wu Y, Shan B, Dai J, Xia Z, Cai J, Chen T *et al*. Dual Role for Inositol-requiring Enzyme 1alpha in Promoting the Development of Hepatocellular Carcinoma during Diet-induced Obesity. Hepatology 2018.

52 You Y, Zheng Q, Dong Y, Xie X, Wang Y, Wu S *et al*. Matrix stiffness-mediated effects on stemness characteristics occurring in HCC cells. Oncotarget 2016; 7: 32221-32231.

53 Zhang R, Lin XH, Ma M, Chen J, Chen J, Gao DM *et al*. Periostin involved in the activated hepatic stellate cells-induced progression of residual hepatocellular

carcinoma after sublethal heat treatment: its role and potential for therapeutic inhibition. J Transl Med 2018; 16: 302.

Figure legends

Fig. 1. Inhibiting IRE1α reduces tumor burden *in vivo*. *(A)* Number of tumors, ***(B)*** size of tumors and ***(C)*** tumor burden of mice with DEN-induced HCC treated with 4μ8C or vehicle-treated controls. ***(D)*** Representative images of H&E- stained liver slides ***(E)*;** Sirius red stained liver slides ***(F)*** and liver slides stained with αSMA-antibodies. ***(G)*** Quantification of percentage of collagen and ***(H)*** αSMA on liver slides. ***(I)*** mRNA-expression of the proliferation marker PCNA in tumor and surrounding non-tumoral liver tissue. P-values were calculated via the Student´s T-test, scale bars = 120μm (D&E) or 50μm (F).

Fig. 2. Tumor cells secrete factors that induce ER-stress in stellate cells, which contributes to their activation. *(A)* mRNA-expression of ER-stress markers CHOP, ***(B)*** spliced XBP1, (***C)*** BiP in stellate cells (LX2) co-cultured with cancer cells (HepG2 or Huh7) and treated with 4μ8C or control. **(D)** Detection of spliced (XBP1s) and unspliced XBP1 (XBP1u) visualized by digestion of XBP1u by *Pst-I.* (***E)*** Images of LX2-cells and HepG2 or Huh7-cells stained with antibodies against BiP. (***F)*** mRNA-expression of stellate cell activation markers αSMA and (***G)*** collagen in LX2-cells co-cultured with HepG2 or Huh7-cells and treated with or without 4μ8C. P-values were calculated via the Student´s T-test.

Fig. 3. Inhibiting IRE1α decreases stellate cell activation in human liver 3D scaffolds engrafted with stellate cells and tumor cells. *(A)* Representative images of H&E and Sirius red stained slides of decellularized human liver scaffolds engrafted with LX2 stellate cells and HepG2-tumor cells treated with 4μ8C or control. ***(B)*** mRNA-expression of the stellate cells activation markers αSMA and ***(C)*** CTGF in liver scaffolds engrafted with stellate cells (LX2) and cancer cells (HepG2), treated with 4μ8C or control. ***(B)*** mRNA-expression of the stellate cells activation marker collagen and ER-stress markers BiP, spliced XBP-1 (XBP1-S) and CHOP in liver scaffolds engrafted with stellate cells (LX2) and cancer cells (HepG2), treated with 4μ8C or control. P-values were calculated via the Student´s T-test, n = 3 samples for each condition, scalebars = 100μm.

Fig. 4. Inhibition of IRE1α decreases tumor cell proliferation. ***(A)*** PCNA mRNA-expression of HepG2 or Huh7-cells grown with LX2-cells and treated with the IRE1α-inhibitor 4μ8C or control. ***(B)*** Relative cell number of LX2 and HepG2 or ***(C)*** LX2 and Huh7-cells treated with 4μ8C or control. ***(D)*** Representative images of tumor cells (HepG2 or Huh7) and LX2-stellate cells stained with antibodies against the HCC-marker Epcam and the proliferation marker ki67. ***(E)*** Cell proliferation of HepG2 or HepG2+LX2 spheroids and ***(F)*** Huh7 or Huh7+LX2 spheroids treated with 4μ8C or control. P-values were calculated via the Student´s T-test, scale bars = 50μm.

Fig. 5. Inhibition of IRE1α decreases cell proliferation and improves liver function in human liver scaffolds engrafted with stellate cells and tumor cells. ***(A)*** PCNA and ***(B)*** Hnf4a expression of human liver scaffolds engrafted with HepG2-tumor cells and LX2-stellate cells, treated with 4μ8C or control. ***(C)*** Representative images of tumor cells (HepG2) and LX2-stellate cells stained with antibodies against the HCC-marker Epcam and the proliferation marker ki67. P-values were calculated via the Student´s T-test, scale bars = 100μm.

Fig. 6. Inhibition of IRE1α decreases cell migration. ***(A)*** mRNA-expression of pro-metastatic markers MMP9 and ***(B)*** MMP1 in HepG2 and Huh7-cells co-cultured with LX2-cells and treated with 4μ8C or control. ***(C)*** Scratch wound on HepG2-cells and LX2-cells treated with 4μ8C or control. ***(D)*** Images of Cell Tracker stained HepG2-cells (Green) and LX2-cells (Red) invading the scratch area. ***(E)*** Quantification of wound size in HepG2-cells and LX2-cells treated with 4μ8C or control. ***(F)*** Number of HepG2-cells and LX2-cells invading the scratch wound after 24h in co-cultures and ***(G)*** mono-cultures. P-values were calculated via the Student´s T-test, scale bars = 120μm.

Fig. 7. Silencing IRE1α in LX2-cells mimics 4μ8C. ***(A)*** IRE1α-mRNA-expression of LX2-cells transfected with IRE1α-siRNA (si-IRE1α), mock-transfected (Scr) or untransfected (Ctrl). ***(B)*** PCNA-mRNA-expression of HepG2-cells co-cultured with IRE1α-silenced LX2-cells or controls ***(C).*** Relative cell numbers in co-cultures of HepG2-cells and IRE1α-silenced LX2-cells or controls. ***(D)*** Proliferation of spheroids of HepG2-cells and IRE1α-silenced LX2-cells or controls ***(E)*** Images and ***(F)*** quantification of αSMA-stained spheroids with HepG2-cells and IRE1α-silenced LX2-cells or controls.

(G) Images and ***(H)*** quantification of scratch wound of HepG2-cells co-cultured with IRE1α-silenced LX2-cells or controls. P-values were calculated via the Student´s T-test, scale bars = 50µm (E) or 120µm (G).

Supplementary figure 1. Activation of the unfolded protein response is mainly located in the stroma of mice with HCC*. (A)* mRNA-expression of the ER-stress marker BiP in tumor and surrounding non-tumoral liver tissue in mice with DEN-induced HCC treated with or without the IRE1α-inhibitor 4µ8C or healthy mice. ***(B)*** Quantification of p-IRE1α staining on liver tissue. ***(C)*** Co-staining of liver tissue with antibodies against αSMA and p-IRE1α. ***(D)*** Co-staining of liver tissue with antibodies against αSMA and BiP. P-values were calculated via the Student´s T-test, scale bars = 50µm.

Supplementary figure 2. Activation of the unfolded protein response pathway is increased in patients with fibrotic HCC. *(A)* Heat map showing ene-set enrichment analysis results from samples from fibrous HCC versos non-fibruous HCC. ***(C)*** Immunohistochemically stained liver biopsies from HCC-patients, using antibodies against IRE1α-mediated actors of the unfolded protein response: WIPI1, SHC1, PPP2R5B and BiP.

Supplementary figure 3. Studying the interaction between stellate cells and tumor cells using 3D spheroids *(A)* Images of spheroids consisting out of LX2-cells and HepG2 or Huh7-cells stained with antibodies against αSMA and **(B)** the quantification of αSMA staining relative to the nuclear Hoechst staining. ***(C)*** Images of spheroids consisting out of LX2-cells and HepG2 or Huh7-cells stained with antibodies against BiP and **(D)** the quantification of BiP staining relative to Hoechst. P-values were calculated via the Student´s T-test, scalebars = 120µm.

Supplementary Figure 4. Secretion of TGFβ by tumor cells activates stellate cells and induces ER-stress. *(A)* concentration of TGFβ in medium from tumor cells (HepG2 or Huh7) grown in mono-culture or co-cultured with LX2-stellate cells, treated with 4µ8C or control. ***(B)*** concentration of TGFβ in medium from liver scaffolds engrafted with stellate cells ***(C)*** (LX2) and tumor cells (HepG2) treated

with 4µ8C or control. mRNA-expression of the ER-stress markers CHOP, ***(D)*** spliced XBP1, ***(E)*** unspliced XBP1 and ***(F)*** BiP in hepatic stellate cells (LX2) grown as mono-culture or in co-cultures with the cancer cell lines HepG2 and Huh7 treated with the TGFβ receptor inhibitor SB-431541 or control**.** (***G)*** mRNA-expression of stellate cell activation markers αSMA and (***H)*** collagen in LX2-cells grown with HepG2 or Huh7-cells and treated with SB-431541 or control. P-values were calculated via the Student´s T-test.

Supplementary Figure 5. Inhibiting IRE1α decreases chemotaxis. ***(A)*** migration plots of LX2-cells co-cultured with HepG2-cells exposed to an FBS-gradient (increasing towards the right) and treated with control or ***(B)*** 4µ8C ***(C)*** Quantification of total migration and ***(D)*** directional migration of LX2-cells (co-cultured with HepG2-cells) towards an FBS-gradient with or without 4µ8C. ***(E)*** Migration plots of HepG2-cells co-cultured with LX2-stellate cells and exposed to an FBS-gradient and treated with control or ***(F)*** 4µ8C. ***(G)*** Quantification of total migration and ***(H)*** directional migration of HepG2-cells (co-cultured with LX2-cells) towards an FBS-gradient with or without 4µ8C. P-values were calculated via the Student´s T-test.

Table 1: Genes the contributed to the core-enrichment of the GSEA

	Probe	Description				Core enrichm
1	ASNS	asparagine synthetase (glutamine-hydrolyzing) [Source:HG	207	0.940	0.0427	Yes
2	PPP2R5B	protein phosphatase 2 regulatory subunit B'beta [Source:H	423	0.821	0.0786	Yes
3	CCL2	C-C motif chemokine ligand 2 [Source:HGNC Symbol;A	847	0.689	0.0986	Yes
4	EXOSC9	exosome component 9 [Source:HGNC Symbol;Acc:HGN	1004	0.654	0.1278	Yes
5	WIPI1	WD repeat domain, phosphoinositide interacting 1 [Sourc	1022	0.649	0.1626	Yes
6	KDELR3	KDEL endoplasmic reticulum protein retention receptor 3	1106	0.635	0.1938	Yes
7	SHC1	SHC adaptor protein 1 [Source:HGNC Symbol;Acc:HGN	2691	0.432	0.1513	Yes
8	TPP1	tripeptidyl peptidase 1 [Source:HGNC Symbol;Acc:HGN	2884	0.414	0.1659	Yes
9	HDGF	heparin binding growth factor [Source:HGNC Symbol;Ac	3235	0.386	0.1724	Yes
10	TLN1	talin 1 [Source:HGNC Symbol;Acc:HGNC:11845]	3264	0.384	0.1921	Yes
11	EXTL3	exostosin like glycosyltransferase 3 [Source:HGNC Symb	3488	0.365	0.2028	Yes
12	TSPYL2	TSPY like 2 [Source:HGNC Symbol;Acc:HGNC:24358]	3680	0.350	0.2139	Yes
13	MBTPS1	membrane bound transcription factor peptidase, site 1 [So	3996	0.327	0.2186	Yes
14	PDIA5	protein disulfide isomerase family A member 5 [Source:H	4530	0.294	0.2125	Yes
15	DCTN1	dynactin subunit 1 [Source:HGNC Symbol;Acc:HGNC:2	4638	0.287	0.2237	Yes
16	DNAJC3	DnaJ heat shock protein family (Hsp40) member C3 [Sou	4761	0.281	0.2339	Yes
17	SULT1A4	sulfotransferase family 1A member 4 [Source:HGNC Sym	4938	0.272	0.2414	Yes
18	PARN	poly(A)-specific ribonuclease [Source:HGNC Symbol;Acc	5037	0.266	0.2519	Yes
19	ADD1	adducin 1 [Source:HGNC Symbol;Acc:HGNC:243]	5375	0.250	0.2514	Yes
20	ERN1	endoplasmic reticulum to nucleus signaling 1 [Source:HG	5411	0.248	0.2635	Yes

Supplementary Table 1. Primer sequences

Supplementary methods 1: histology and immunohistochemistry

Figure 1

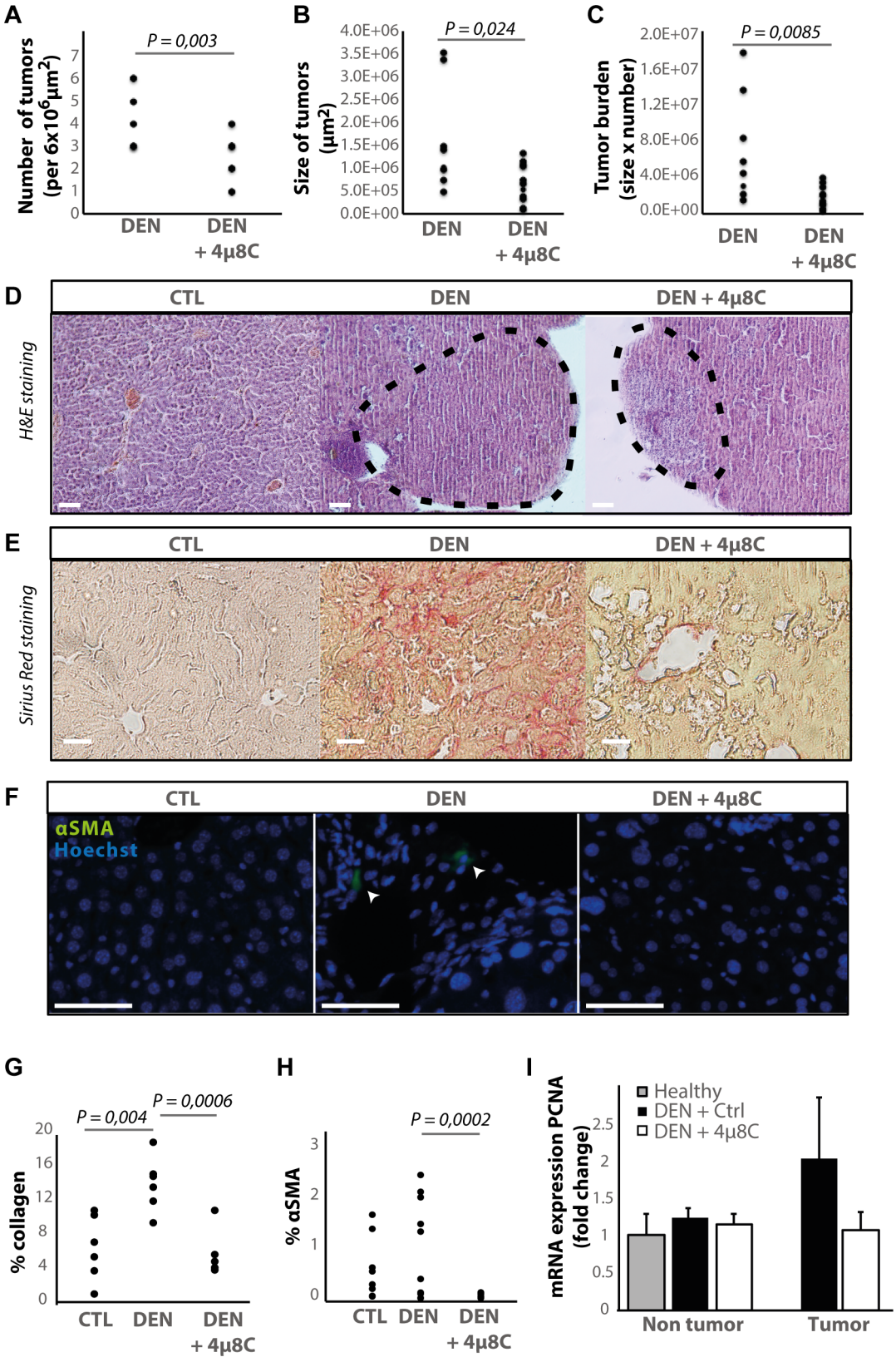
A
Number of tumors (per 6x10^6µm^2)
P = 0,003
DEN
DEN + 4µ8C
B
Size of tumors (µm^2)
P = 0,024
C
Tumor burden (size x number)
P = 0,0085
D
CTL
DEN
DEN + 4µ8C
H&E staining
E
Sirius Red staining
F
αSMA
Hoechst
G
% collagen
P = 0,004
P = 0,0006
H
% αSMA
P = 0,0002
I
mRNA expression PCNA (fold change)
Healthy
DEN + Ctrl
DEN + 4µ8C
Non tumor
Tumor

Figure 2

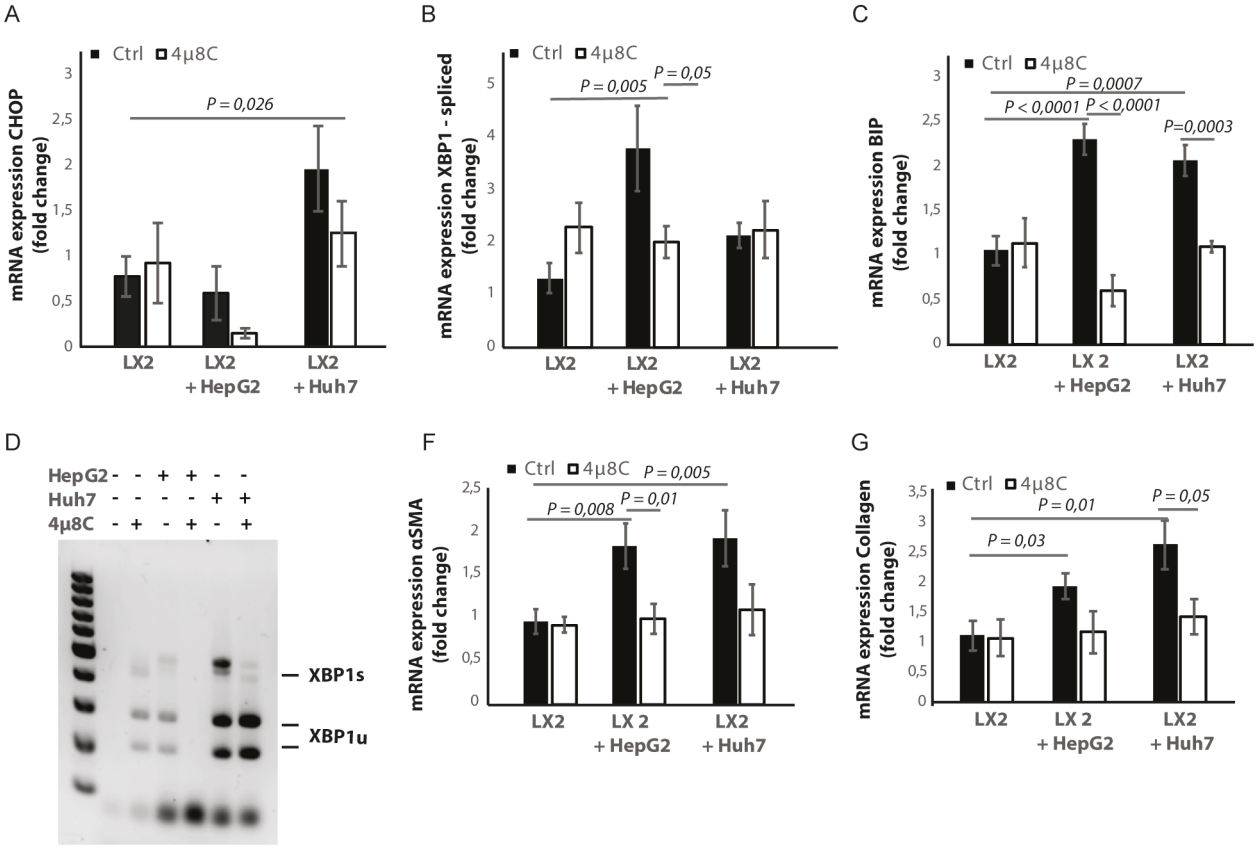
A
Ctrl
4µ8C
mRNA expression CHOP (fold change)
P = 0,026
LX2
LX2 + HepG2
LX2 + Huh7
B
mRNA expression XBP1 - spliced (fold change)
P = 0,005
P = 0,05
C
mRNA expression BIP (fold change)
P = 0,0007
P < 0,0001
P < 0,0001
P=0,0003
LX 2 + HepG2
D
HepG2
Huh7
4µ8C
XBP1s
XBP1u
F
mRNA expression αSMA (fold change)
P = 0,005
P = 0,008
P = 0,01
G
mRNA expression Collagen (fold change)
P = 0,01
P = 0,05
P = 0,03

Figure 3

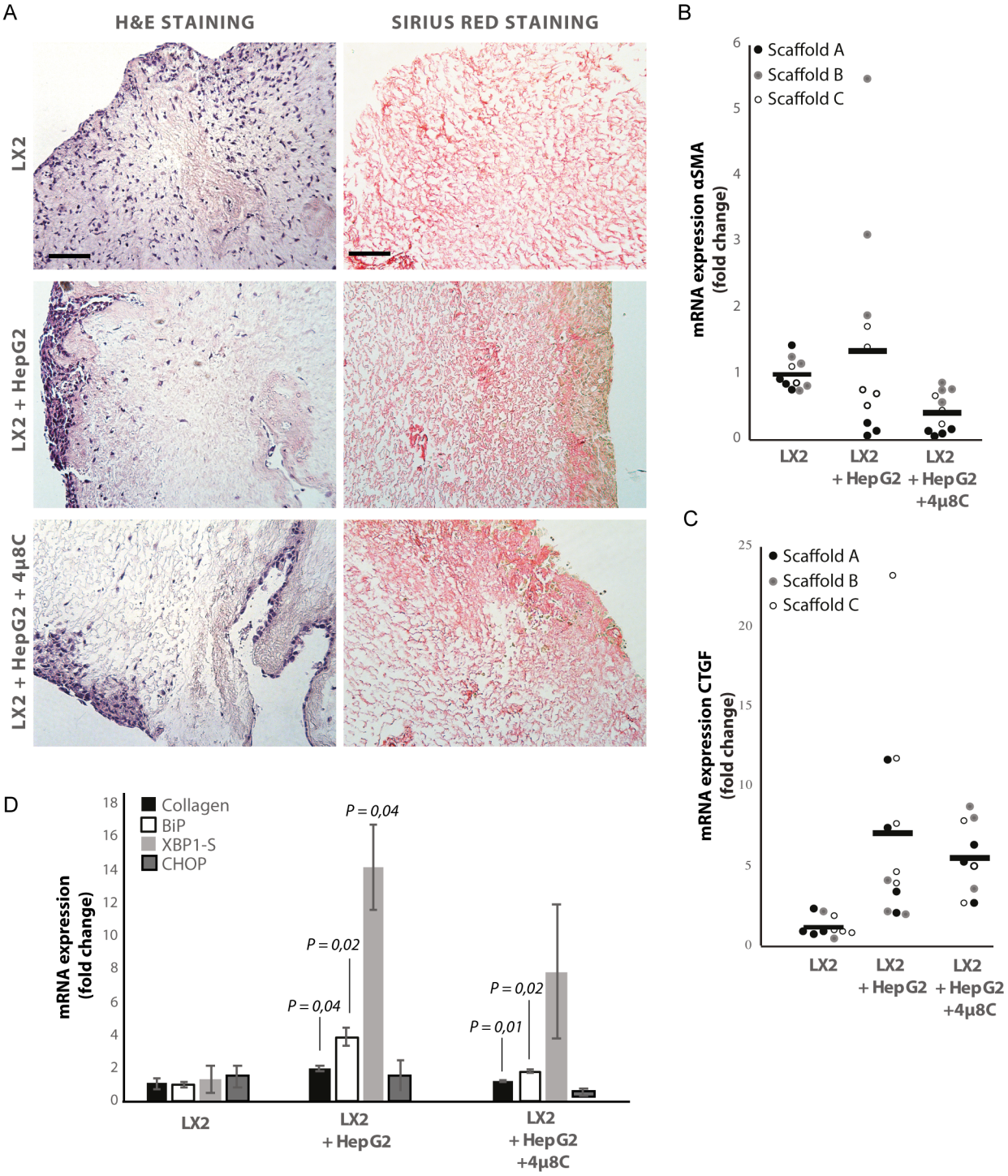
A
H&E STAINING
SIRIUS RED STAINING
LX2
LX2 + HepG2
LX2 + HepG2 + 4µ8C
B
Scaffold A
Scaffold B
Scaffold C
mRNA expression αSMA (fold change)
0
1
2
3
4
5
6
LX2
LX2 + HepG2
LX2 + HepG2 +4µ8C
C
Scaffold A
Scaffold B
Scaffold C
mRNA expression CTGF (fold change)
0
5
10
15
20
25
LX2
LX2 + HepG2
LX2 + HepG2 +4µ8C
D
Collagen
BiP
XBP1-S
CHOP
mRNA expression (fold change)
0
2
4
6
8
10
12
14
16
18
P = 0,04
P = 0,02
P = 0,04
P = 0,02
P = 0,01
LX2
LX2 + HepG2
LX2 + HepG2 +4µ8C

Figure 4

A

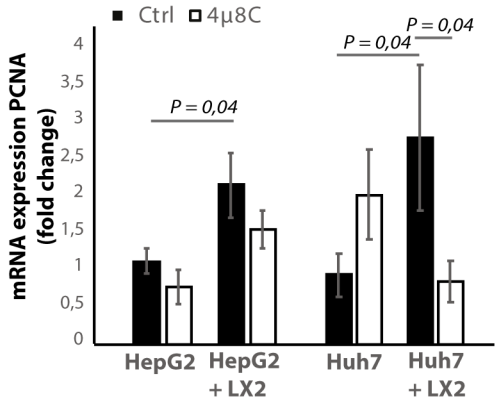

B

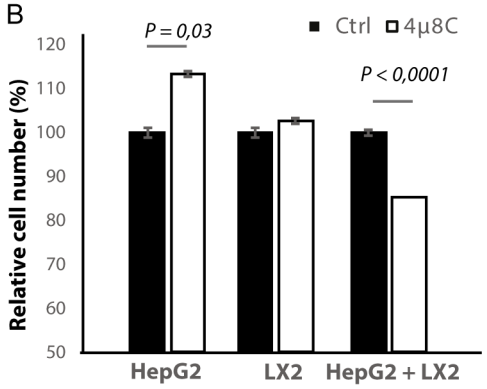

C

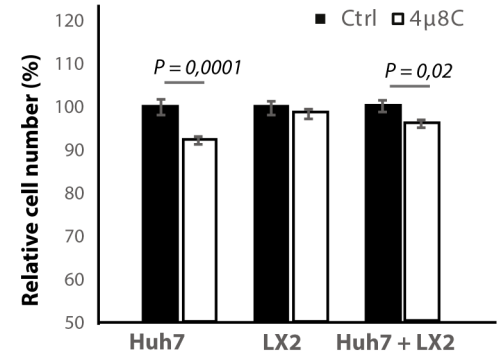

D

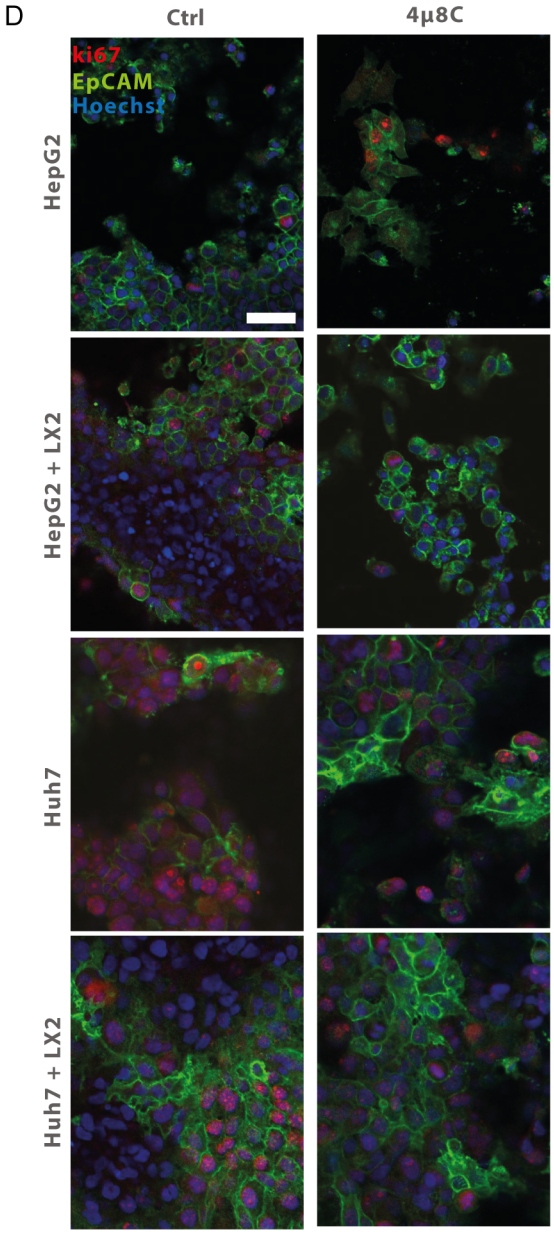

E

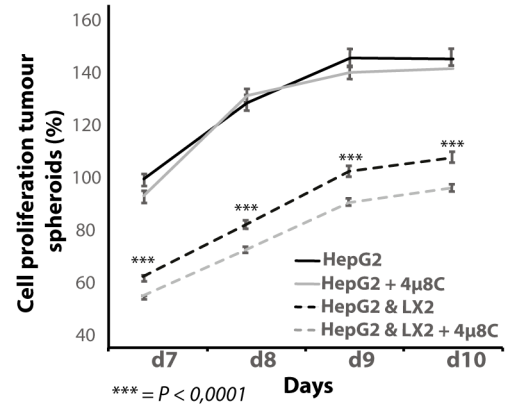

F

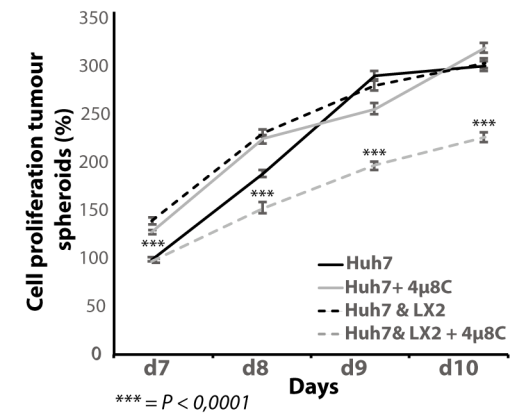

Figure 5

A

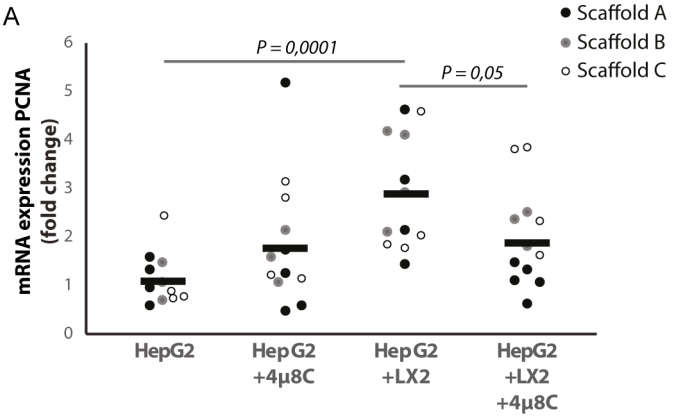
Scaffold A
Scaffold B
Scaffold C
P = 0,0001
P = 0,05
mRNA expression PCNA (fold change)
0
1
2
3
4
5
6
HepG2
HepG2 +4µ8C
HepG2 +LX2
HepG2 +LX2 +4µ8C

B

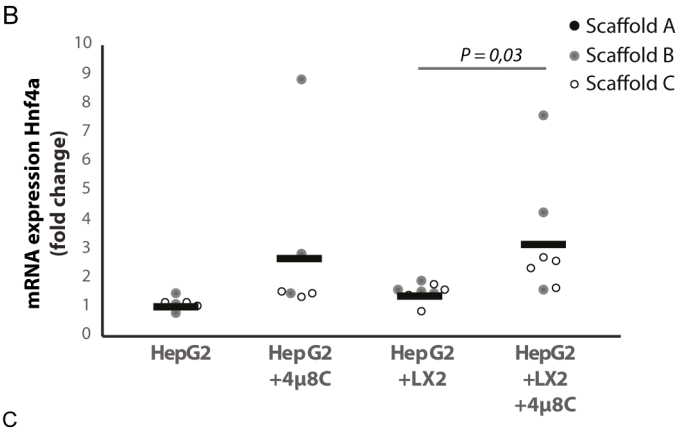
Scaffold A
Scaffold B
Scaffold C
P = 0,03
mRNA expression Hnf4a (fold change)
0
1
2
3
4
5
6
7
8
9
10
HepG2
HepG2 +4µ8C
HepG2 +LX2
HepG2 +LX2 +4µ8C

C

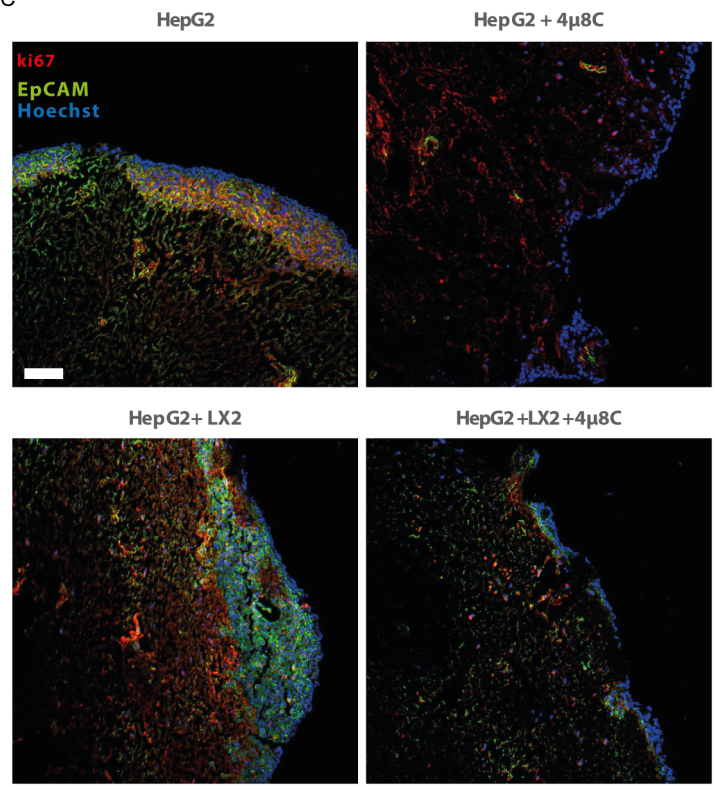
HepG2
HepG2 + 4µ8C
ki67
EpCAM
Hoechst
HepG2+ LX2
HepG2 +LX2 +4µ8C

Figure 6

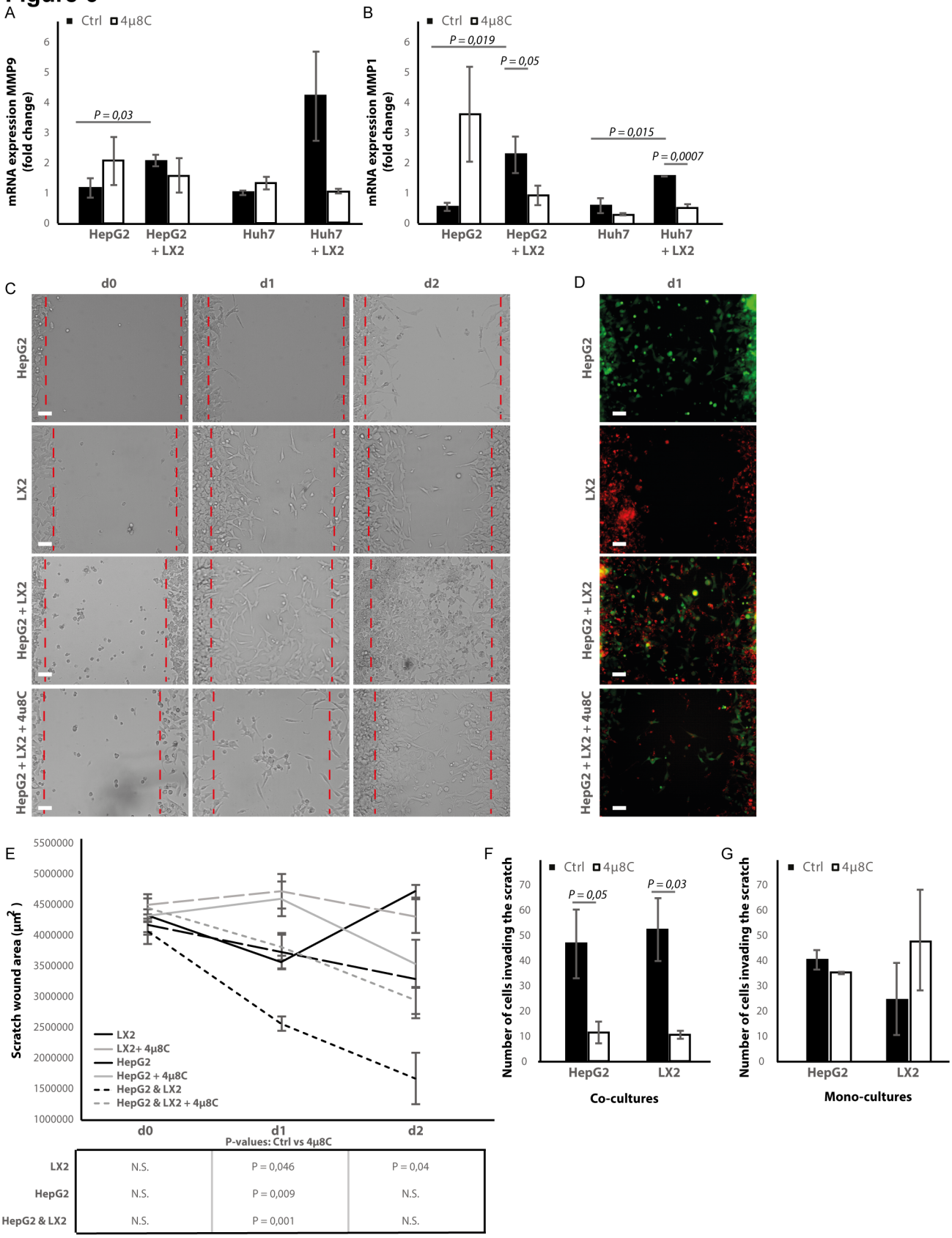

P-values: Ctrl vs 4µ8C

	d0	d1	d2
LX2	N.S.	P = 0,046	P = 0,04
HepG2	N.S.	P = 0,009	N.S.
HepG2 & LX2	N.S.	P = 0,001	N.S.

Figure 7

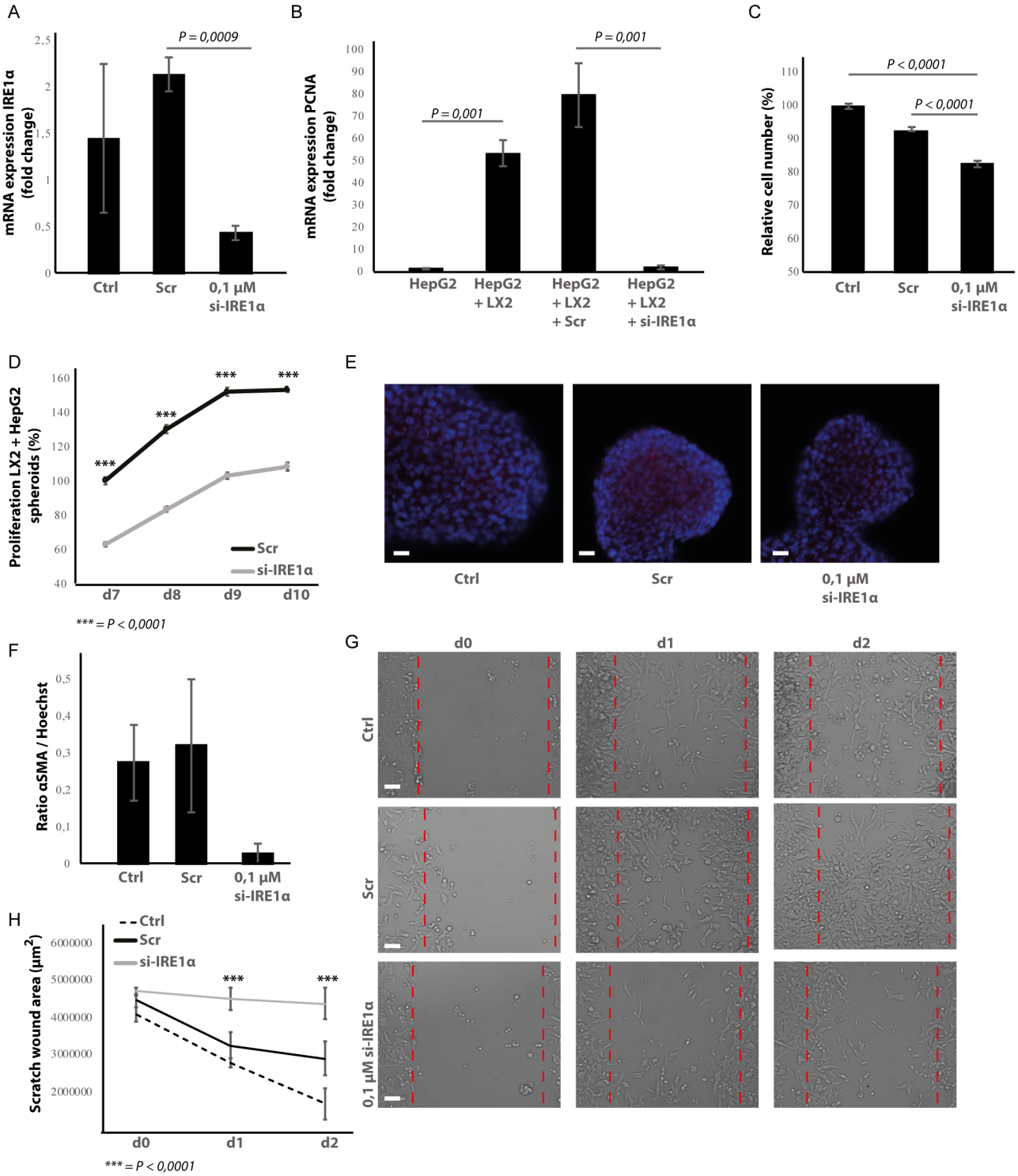
A
mRNA expression IRE1α (fold change)
P = 0,0009
Ctrl
Scr
0,1 µM si-IRE1α
B
mRNA expression PCNA (fold change)
P = 0,001
P = 0,001
HepG2
HepG2 + LX2
HepG2 + LX2 + Scr
HepG2 + LX2 + si-IRE1α
C
Relative cell number (%)
P < 0,0001
P < 0,0001
Ctrl
Scr
0,1 µM si-IRE1α
D
Proliferation LX2 + HepG2 spheroids (%)
***
Scr
si-IRE1α
d7
d8
d9
d10
*** = P < 0,0001
E
Ctrl
Scr
0,1 µM si-IRE1α
F
Ratio αSMA / Hoechst
Ctrl
Scr
0,1 µM si-IRE1α
G
d0
d1
d2
Ctrl
Scr
0,1 µM si-IRE1α
H
Scratch wound area (µm²)
Ctrl
Scr
si-IRE1α
***
d0
d1
d2
*** = P < 0,0001